INTERNATIONAL JOURNAL FOR NUMERICAL METHODS IN FLUIDS
Int. J. Numer. Meth. Fluids **30**: 725–742 (1999)

VARIABLE DENSITY FLOW IN POROUS MEDIA. A STUDY BY MEANS OF PORE LEVEL NUMERICAL SIMULATIONS

A. BOUHOUCH, M. PRAT* AND H. BOISSON

Institut de Mécanique des Fluides de Toulouse, UMR CNRS—INP/UPS No. 5502, Avenue du Professeur Camille Soula, 31400 Toulouse, France

SUMMARY

This paper is devoted to the modelling of isothermal low Reynolds and Mach numbers transient compressible flow through porous media. Traditionally, this type of flow at the macroscopic level is described by the classical Darcy's law combined with a mass balance that includes the transient term. This model is called the 'classic model'. The aim of this paper is to explore the validity of this classic model. To this end, the flow of an ideal gas is considered within two-dimensional model porous media. The flow is due to the imposed pressure variations at the outlet of the fluid domain. At the microscopic level, the flow is computed by solving the full compressible Navier–Stokes equations in two dimensions. Special attention is given to the outlet boundary conditions. The analysis is based on the comparison between the macroscopic data, obtained on the one hand by spatially averaging the microscopic results, and on the other hand by solving the problem directly at the macroscopic level. Situations for which a good agreement is found between the two series of data and situations for which discrepancies are observed are exhibited. These various behaviours are discussed in terms of the various time scales controlling the flow and are explained by analysing the flow structure at pore level. Copyright © 1999 John Wiley & Sons, Ltd.

KEY WORDS: porous media; compressible flow; PISO algorithm; Navier–Stokes equations; open boundary conditions

1. INTRODUCTION

Compressible or variable density flows in porous media have been studied much less in comparison with the huge literature devoted to incompressible flows. However, there is a large variety of situations in which variable density or compressible flows in porous media may be encountered. Initial studies (see Scheidegger [1] and references therein) were motivated by modelling oil or gas production in reservoirs. More recent applications involving compressible flows in porous media include the aeration of cereal stores, De Ville [2], the erosion of concrete airfield pavements by jet exhausts, Kodres [3], gas fields or coal dust explosions, Auriault [4], storage of thermal energy in packed beds, Sozen and Vafai [5] and separation process of gas

* Correspondence to: Institut de Mécanique des Fluides de Toulouse, UMR CNRS—INP/UPS No. 5502, Avenue du Professeur Camille Soula, 31400 Toulouse, France. E-mail: prat@imft.fr

Contract/grant sponsor: CNES (Centre National d'Etudes Spatiales)
Contract/grant sponsor: ESA (European Space Agency)
Contract/grant sponsor: CNRS

CCC 0271–2091/99/140725–18$17.50

Received January 1998
Revised August 1998

mixture, Raghavan *et al.* [6]. As far as the authors are concerned, the motivation for the present work was the study of flow and heat transfer within external thermal protections of hypersonic space vehicles, Bouhouch *et al.* [7]. One may also distinguish various classes of compressible flows. Most of the compressible flows in porous media are in fact low Mach number flows. These are generally slightly compressible flows and in many cases, it would be more appropriate to term them variable density flows. However, there has been also some studies on truly compressible flows in porous media (Shreeve [8], Emanuel and Jones [9]). This case poses an interesting modelling problem, as discussed by Nield [10], and certainly deserves further investigations. Another class of flow touching the issue of compressible flows in porous media is acoustics in porous media. This class has been extensively studied (see for instance Johnson *et al.* [11]). As far as the current authors are concerned, they limit their investigation to the slightly compressible flow class. Furthermore, they shall only consider cases for which temperature variations are negligible. For modelling this type of flow at the macroscopic level, the classic approach relies on Darcy's law combined with a mass balance equation, including a transient term, Scheidegger [1]. The main objective of the present paper is to assess the validity of this classic model. To this end, numerical simulations of flows at pore level have been carried out for two types of model porous medium. Macroscopic data are obtained by spatially averaging the pore level simulation date. The analysis is based on comparison between the spatially averaged data and the data obtained directly at the macroscopic level by solving the classic macroscopic model. Cases for which a good agreement is obtained between the two series of data and also cases for which the classic macroscopic model is clearly non-valid are exhibited. It is shown that the latter cases correspond to situations for which the flow is not quasi-steady at pore level. The particular flows considered in this study are generated by pressure variations at an exit boundary, typically a 'rapid' pressure decrease or a 'rapid' pressure increase.

2. MODEL FORMULATION

2.1. Assumptions

For the present effort, the following assumptions were made: quasi-isothermal low Reynolds and Mach numbers transient flows are assumed. These imply that heat transfer can be

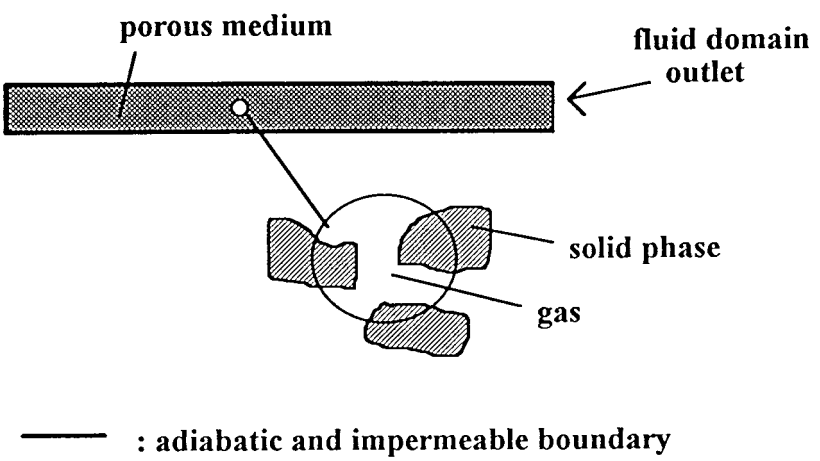

Figure 1. Physical under study.

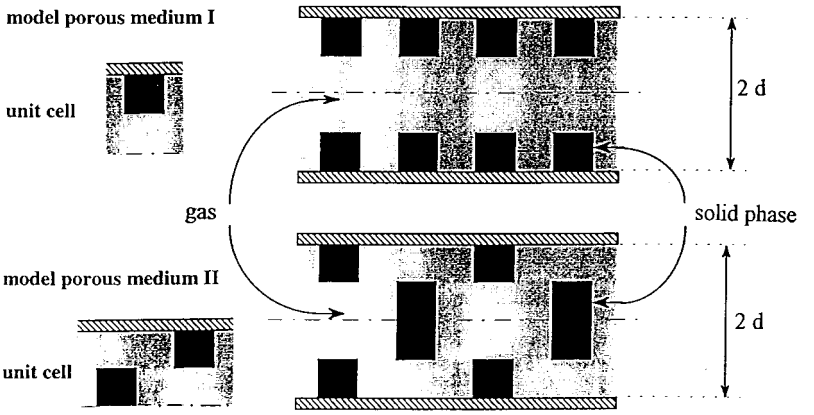

Figure 2. Model porous media.

neglected at the macroscopic level. The physical situation under study is depicted in Figure 1. Initially, the gas within the porous medium is at rest, the gas pressure and temperature are uniform and equal to the external pressure and temperature. At $t > 0$, the external pressure decreases and thereby induces the gas flow within the porous medium. The gas leaves the porous medium through the open boundary of the porous domain (Figure 1). In the present study, the range of pressure variation is such that the mean free path of the gas molecules is always significantly lower than the pore size, i.e. the flow at the pore level can be simulated by the Navier–Stokes equations with no-slip conditions at the solid walls. At the pore level model porous media consisting of two-dimensional arrangements of square cylinders were considered, Figure 2. Unit cells are also depicted in Figure 2 (note that the definition of the unit cell takes into account the symmetry of the domain). The solid surface fraction is 25% for both models, i.e. the porosity is 75%. A typical computational domain at the pore level is shown in Figure 3. As can be seen from Figure 3, the domain is of limited extension in the y-direction and of the spatially periodic type in the x-direction. Typically, the extension in the x-direction represents 50 unit cells. This is assumed to be sufficient to ensure length scale separation (see Section 2.4). The fluid domain is limited by an impermeable solid boundary at $x = 0$. At $x = L$, there is the open boundary from which the fluid can leave the pore space when the external pressure decreases.

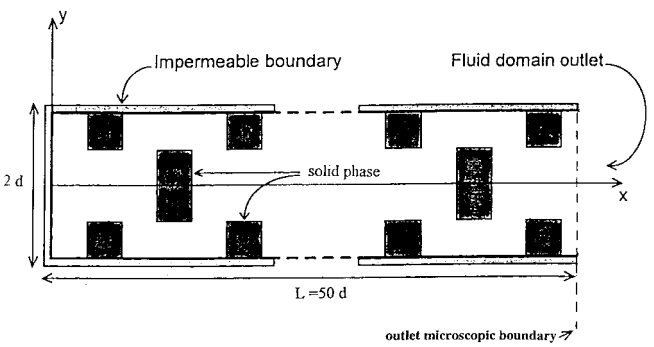

Figure 3. Typical computational domain and location of the microscopic boundary at $x = L$.

2.2. Macroscopic model

Traditionally, this type of flow at the macroscopic level is described by the classical Darcy's law combined with a mass balance that includes the transient term. This model, called the 'classic model' in the following and written hereafter for a one-dimensional geometry, since the problem under study is one-dimensional at the macroscopic level, reads

$$U = -\frac{k}{\mu}\frac{\mathrm{d}P}{\mathrm{d}x}, \tag{1}$$

$$P = \rho r T, \tag{2}$$

$$\frac{\partial P}{\partial t} = \frac{\mathrm{d}}{\mathrm{d}x}\left(\frac{Pk}{\mu\varepsilon}\frac{\mathrm{d}P}{\mathrm{d}x}\right), \tag{3}$$

in which P is the pressure, T is the temperature, ρ is the gas density, U is the Darcy velocity, k is the permeability of the medium, μ is the gas viscosity, ε is the porosity, $r = R/M$ with R gas constant and M the fluid molecular weight.

The initial and boundary conditions are

$$t = 0, \qquad P = p_0, \quad \forall x, \tag{4}$$

$$t > 0, \qquad \frac{\mathrm{d}P}{\mathrm{d}x} = 0 \ \text{ at } \ x = 0, \tag{5}$$

$$P = f(t) \ \text{ at } \ x = L, \tag{6}$$

where $f(t)$ is an imposed pressure variation law.

2.3. Pore level model

At the microscopic (or pore) level, the flow is computed by solving the fully compressible Navier–Stokes equations over a domain containing several pores. The equations to be solved read (in a Cartesian system of co-ordinates x_i, x_j, x_k)

$$\frac{\partial \rho}{\partial t} + \frac{\partial m_i}{\partial x_i} = 0, \tag{7}$$

$$\frac{\partial e}{\partial t} + \frac{\partial}{\partial x_i}((e+p)u_i) = \frac{\partial}{\partial x_i}(u_j\tau_{ij}) - \frac{\partial q_i}{\partial x_i}, \tag{8}$$

$$\frac{\partial m_i}{\partial t} + \frac{\partial}{\partial x_j}(m_i u_j) + \frac{\partial p}{\partial x_i} = \frac{\partial \tau_{ij}}{\partial x_j}, \tag{9}$$

in which

$$e = \frac{1}{2}\rho u_i u_i + \frac{p}{\gamma - 1}, \tag{10}$$

$$m_i = \rho u_i, \tag{11}$$

$$\tau_{ij} = \mu\left(\frac{\partial u_i}{\partial x_j} + \frac{\partial u_j}{\partial x_i} - \frac{2}{3}\delta_{ij}\frac{\partial u_k}{\partial x_k}\right), \tag{12}$$

where p is the pressure, m_i (resp. m_j, m_k) is the momentum density in the i- (resp. j-, k-) direction, e is the total energy density, $q_i = -\lambda(\mathrm{d}T/\mathrm{d}x_i)$ is the heat flux in the i-direction (and similar definitions in the j- and k-directions); x_i (resp. x_j, x_k) is the co-ordinate in the i- (resp.

j-, k-) direction, u_i (resp. u_j, u_k) is the velocity component in the i- (resp. j-, k-) direction, λ is the fluid thermal conductivity, γ the ratio of specific heats.

As for the macroscopic model, it is assumed that the gas behaves as an ideal gas,

$$p = \rho RT. \tag{13}$$

The initial boundary conditions are (hereafter, as the problem considered in the following is two-dimensional at the pore level, x and y are used for denoting the spatial Cartesian co-ordinates, see Figure 3)

$$t = 0, \qquad p = p_0; \qquad T = T_0, \qquad \mathbf{u} = (0, 0), \quad \forall (x, y), \tag{14}$$

$$t > 0, \quad u = (0, 0), \quad q = (0, 0) \text{ at solid boundaries}, \tag{15}$$

$$P = f(t) \text{ at } x = L \forall y + \text{outlet boundary conditions for } u, \ \rho \text{ and } T. \tag{16}$$

The outlet boundary conditions for u, ρ and T are discussed in Section 3.

2.4. Influence of boundary conditions

As we consider media with only a rather limited number of unit cells, one may question the relevance of Darcy's law in the present context. For instance within the framework of the homogenisation method (Sanchez-Palencia [12]), Darcy's law is obtained formally in the limit of an extremely small ration between the pore length scale d (the size of a unit cell in this system) and the macroscopic length scale (L with the current notations). In fact, this condition is overly restrictive in practice and very often the macroscopic description gives an excellent approximation even for systems containing only a limited number of unit cells, see for instance Prat [13]. However, in such a case, it is necessary to eliminate the errors that may be induced by the macroscopic boundary conditions (Equations (5) and (6) in the problem at hand) if one wants to be in a position to compare macroscopic variables obtained, on the one hand by spatially averaging microscopic results, and on the other hand by solving macroscopic governing equations. From previous studies, Prat [13,14], it is known that a Neumann condition, Equation (5), does not introduce any error, while a Dirichlet condition, Equation (6), may introduce an error of the order of $(d/L)\delta P$ on the determination of the pressure from the macroscopic equation, Equation (3) (δP is the pressure difference between $x = 0$ and $x = L$). Therefore, this error can be significant when the ration d/L is not small, as it is the case in the current simulations. However, as explained in Prat [13], the exact magnitude of the error depends on the location of the microscopic boundary within the first unit cell (at $x = L$ in Figure 3). It follows that the error can be completely eliminated by defining adequately the location of the microscopic boundary. For instance, for model II, it suffices to locate the open microscopic boundary as depicted in Figure 3 for eliminating any error associated with the macroscopic boundary conditions (the error would have been maximum if the outlet microscopic boundary had been located along the right-hand-sides of the solid particles in Figure 3, see Prat [13] for more details). Under these circumstances, it is therefore quite possible to compare average variables deduced from microscopic simulations, based on solving Equations (7)–(16), with the corresponding variables computed by means of the macroscopic model, Equations (1)–(6), even if the system contains only a few tens of unit cells. Care, however, should be taken in defining the averaging operators. This is discussed in Section 4.3.

3. NUMERICAL METHODS

The macroscopic model, Equations (1)–(6), is solved by the Galerkin finite element method. At the macroscopic level, the problem to be solved is in fact one-dimensional. One-dimensional elements and linear interpolation functions were used. Solving the pore level model, Equations (7)–(16), is more involved. Note that the pore level problem is two-dimensional. To this end, a finite volume technique was used. It is based on the pressure-implicit with splitting operators (PISO) algorithm, Issa [15], with rectangular finite volumes and classical staggered grids. This method is well-adapted to solving variable density low Mach flows, such as the ones considered in the present study. This algorithm is described in detail in Issa [15]. Only its main features are recalled here. This is a predictor–corrector algorithm in which the time derivatives are approximated by a first-order Euler forward scheme. The spatial finite volume scheme is the hybrid scheme, Patankar [16]. To progress from a time station t^n to the following one t^{n+1}, fractional time steps are defined. In a first predictor step, the momentum equation (9) is solved with the values of the pressure and the density taken at t^n. The values of the momentum are explicitly updated in a first corrector step, which solves a Poisson-like equation for a pressure correction ensuring approximate mass conservation from Equation (7). Density is then computed via the state equation, Equation (13). A second stage is initiated by a predictor step for the energy equation (8), where the values of pressure, density and momentum are fixed at the previous fractional time step. A new corrector step is then performed on the same principle, i.e. solving a Poisson-like equation coming from the mass conservation equation (7) and updating momentum. This process could be continued to convergence by more predictor–corrector sequences but it is stopped at the end of the first two stages. Indeed, it has been shown by Issa [15] that the order of accuracy obtained after two stages is compatible with the discretisation schemes used. Only the time step is adjusted in order to follow the physical unsteadyness of the phenomenon (the interested readers may refer to Issa [15] or to the textbooks of Patankar [16] or Ferziger and Peric [17]). All the implicit equations for momentum and energy used for the predictor steps are linearised considering that during the change from t^n to t^{n+1}, the transport velocity in the convection operator can be approximated by the velocity at t^n. The whole procedure requires solving six pentadiagonal linear systems for a two-dimensional problem (further details can be found in Bouhouch [18]).

Naturally, appropriate boundary conditions on every face of the computational domain must be prescribed. Imposing the boundary conditions at solid walls or symmetry axis does not pose any particular problem. The outlet boundary conditions are less straightforward. In particular, care must be exercised in specifying the outlet boundary conditions in order to avoid numerical instabilities and to control spurious wave reflections at the computational boundaries. To this end, the Navier–Stokes characteristic boundary conditions (NSCBC) strategy, proposed by Poinsot and Lele [19], were adapted to this problem. In essence, the NSCBC method is based on a local inviscid analysis of the waves crossing the boundary. However, the work of Poinsot and Lele concerned an explicit finite difference method. Care should, therefore, be taken for extending this approach to implicit formulations.

The NSCBC algorithm is implemented for the outflow boundary as follows. The two-dimensional Navier–Stokes, Equations (7)–(9), are modified on the line of the outflow condition. The partial derivative system is linearised in the x-direction considering characteristics of wave propagation. The procedure implies to determine the amplitudes L_i associated with the corresponding eigenvalues ψ_i (also called characteristic celerities) with $\psi_1 = u_x - c$, $\psi_2 = \psi_3 = u_x$ and $\psi_4 = u_x + c$, where c is the celerity of sound waves. For the outflow boundary conditions all positive characteristic unknowns are determined numerically by extrapolating the values

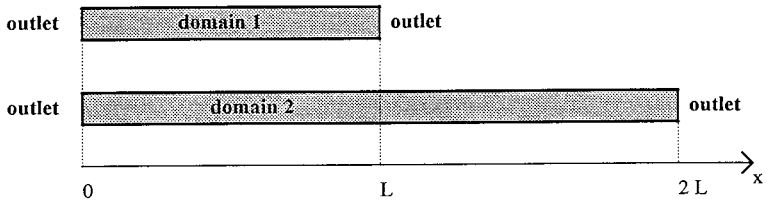

Figure 4. Computational domains for the open boundary condition test.

from inside the domain. The negative ones, for subsonic output, must be specified in order to avoid spurious reflections. Obtained by this method is a dynamical prescription of boundary conditions based on characteristic celerities. In summary, three steps are necessary in order to implement this condition: (1) calculate the characteristic velocities, (2) extrapolate or prescribe appropriate values of the required variables, (3) compute ρ, ρu_x, ρu_y, e on the boundary. The relevance of the NSCBC strategy for deriving open boundary conditions in this problem is illustrated hereafter. With the same version of the PISO algorithm, this method was also tested in the case of an unsteady vortex motion, Hannoun *et al.* [20], and provided fully satisfactory results for the outflow of vorticity as well as for an entropy wave.

4. SIMULATIONS

This section presents the results of the various numerical simulations performed. Firstly, the validity of the open boundary conditions discussed above is demonstrated through a numerical test (Section 4.1). Next, Section (4.2) is devoted to a short discussion on the optimal grid size. In Section 4.3, the intrinsic permeability for both model porous media are computed. This parameter is a necessary input for the macroscopic model. Then, the last section (Section 4.4), which is the key section of the paper, presents the comparison between the two approaches (spatial averaging of microscopic fields versus direct computation of these fields at the macroscopic level).

4.1. Open boundary condition test

In order to test the validity of the open boundary conditions, the following test case was considered. Computations were carried out for the two domains depicted in Figure 4. As can be seen from Figure 4, the only difference between the two domains is their lengths. The total length is L for domain 1 and $2L$ for domain 2. Open boundaries are assumed at $x = 0$ and $x = L$ for domain 2. The idea is to compare the flows within the two domains at $x = L$ at various times for identical initial conditions. These initial conditions are selected in order to induce a flow within the domain. They are given by

$$p(x) = f_p(x) = p_0\left[1 + \exp\left(\frac{(x - 0.5L)^2}{\alpha}\right)\right] \quad \text{for } 0 \le x \le L,$$
$$p(x) = f_p(L) \quad \text{for } L \le x \le 2L \text{ (domain 2)} \tag{17}$$

$$\rho(x) = f_\rho(x) = \rho_0\left[1 + \exp\left(\frac{(x - 0.5L)^2}{\alpha}\right)\right], \quad 0 \le x \le L, \tag{18}$$

$$\rho(x) = f_\rho(L) \quad \text{for } L \le x \le 2L \text{ (domain 2)}$$

$$u(x) = f_u(x) = u_0\left[1 + \exp\left(\frac{(x - 0.5L)^2}{\alpha}\right)\right], \quad 0 \le x \le L, \tag{19}$$

$$u(x) = f_u(L) \quad \text{for } L \le x \le 2L \text{ (domain 2)}$$

with $p_0 = 100000$ Pa, $\rho_0 = 1.27$ kg m^{-3} and $u_0 = 10$ m s^{-1}. α is a constant equal to 4×10^4. Figure 5 shows the shape of the initial distributions as described by Equations (17)–(19). Note that the flow is one-dimensional. However, the two dimensional version of the code was used with only two nodes in the y-direction. Figure 6 shows the evolution of the pressure distribution at various times for both domains. No undesirable effects are visible in Figure 6. An example of comparison between the solutions at $x = L$ for the two domains is displayed in Figure 7. It can be seen that the two solutions are identical. This illustrates the validity of the procedure used to specify the open boundary conditions in this case. Additional comparisons reported in Bouhouch [18] lead to the same conclusion. In this test, constant step size grids of 56 nodes for domain 1 and 112 nodes for domain 2 were used. The time step was $\Delta t = 37$ μs.

4.2. Grid size independence

A series of test was conducted to determine a satisfactory compromise in terms of number of nodes. For a domain containing 20 unit cells of type I (see Figure 2 for the definition of the unit cell), simulations of a depressurisation process were performed for four different grids (with increasing number of nodes). A linear pressure evolution was imposed at the outlet boundary and comparisons between the velocity profiles at two sections of the computational

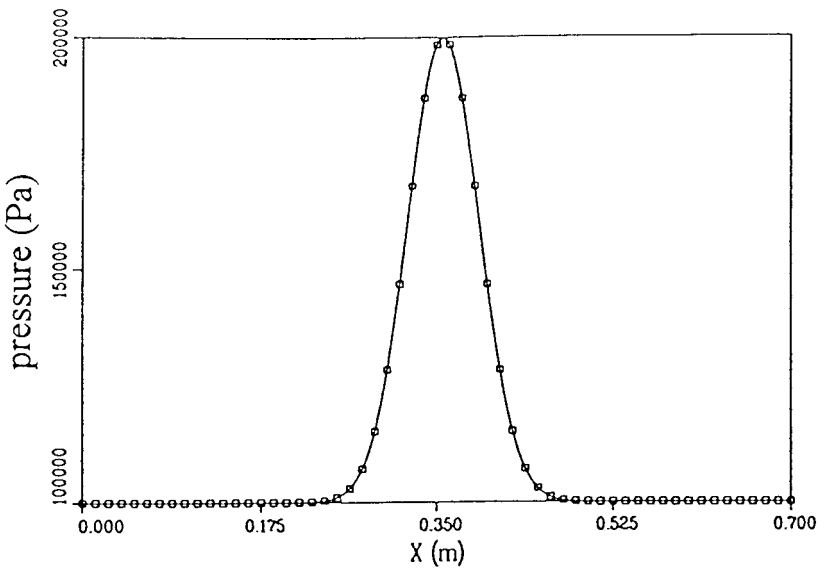

Figure 5. Example of initial condition for the open boundary condition (OBC) test.

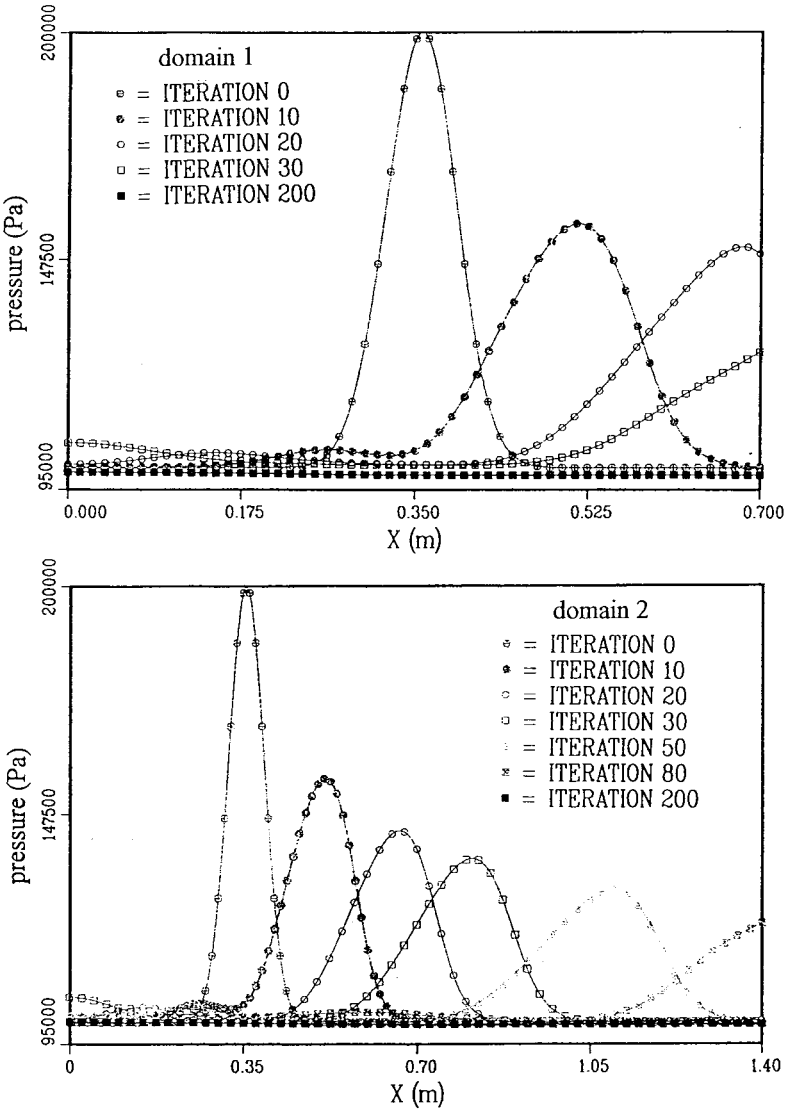

Figure 6. OBC test. Pressure distributions at various times for domain 1 and domain 2.

domain were made at various times. Figure 8 shows a representative example of the results. A grid of 20×20 nodes per half unit was finally considered to be satisfactory for the problem at hand.

4.3. Permeability

Computations with the macroscopic model require the specification of the intrinsic permeability k. To this end the microscopic steady creeping flow was computed over a representative unit cell for each model porous medium (this type of flow was chosen since the validity of Darcy's law at the macroscopic level can be rigorously established for this type of microscopic flow through spatially periodic porous media, see for instance Sanchez-Palencia [12]). Spatially

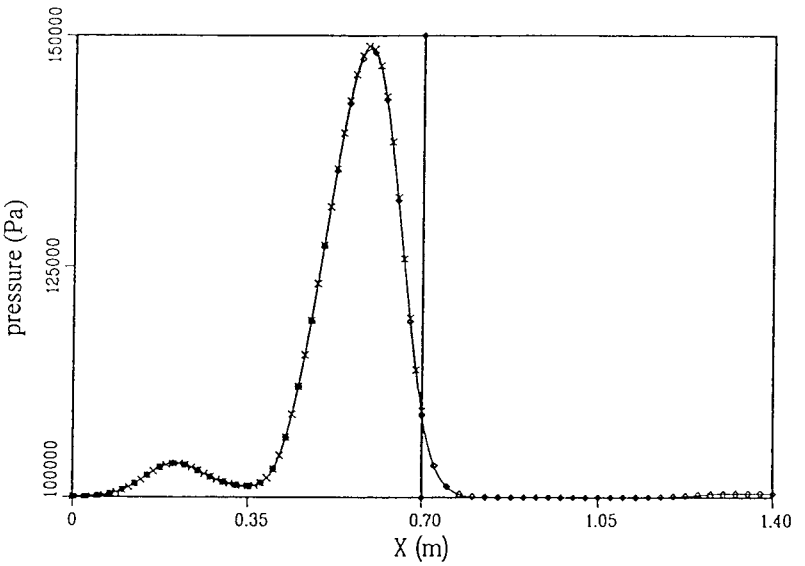

Figure 7. OBC test. Comparison of pressure distributions at $t = 15\Delta t$. × solution for domain 1. ◇ solution for domain 2.

periodic boundary conditions in the x-direction were imposed for these computations. Figure 9 shows the flow structure obtained for model porous medium I. As can be seen from Figure 9, the flow is characterised by recirculating eddies. It is interesting to note that the eddies are symmetrical about a y-axis crossing the cavities in their middle. This result is fully consistent with the results obtained for creeping flows over cavities, see e.g. Higdon [21]. The permeability is then determined by using Darcy's law,

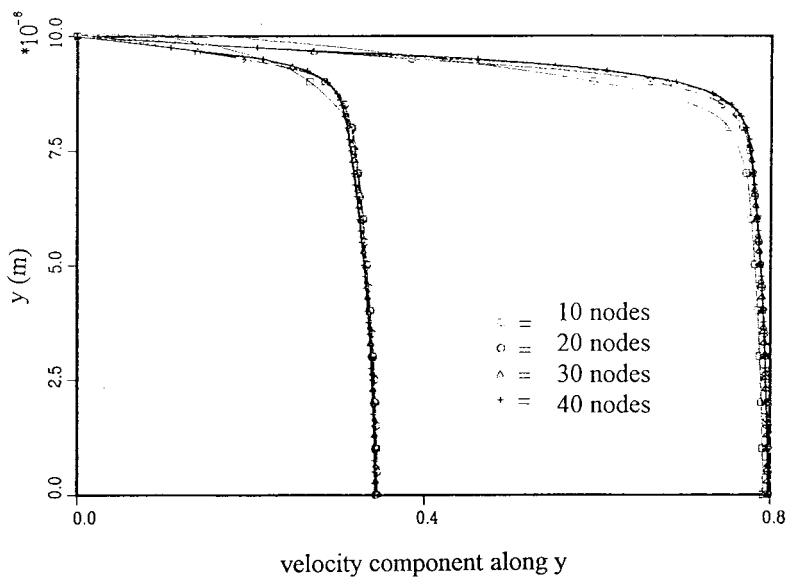

Figure 8. Grid independence test. Example of results.

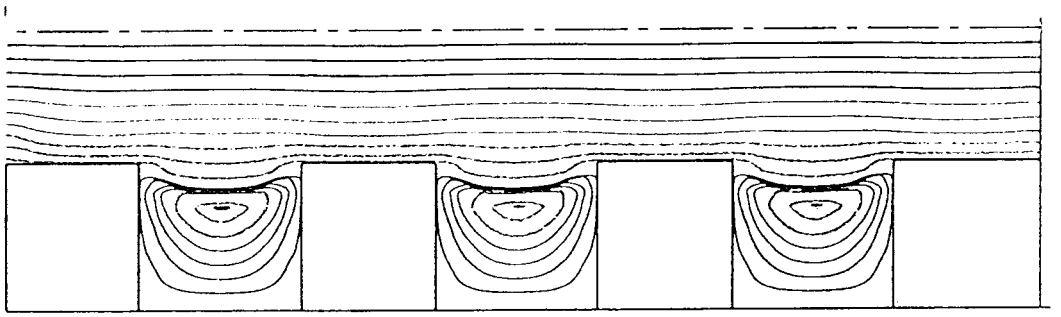

Figure 9. Steady state incompressible creeping flow structure at pore level for model porous medium I (streamline pattern).

$$k = -\frac{\mu \langle u_x \rangle}{\partial \bar{p}/\partial x}, \tag{20}$$

where $\langle u_x \rangle$ is the spatial phase average of the microscopic velocity component in the x-direction and $\bar{p}$ is the cellular average of the microscopic pressure defined as follows,

$$\langle u_x \rangle = \frac{1}{V} \int_{V_f} u_x \, \mathrm{d}V, \tag{21}$$

$$\bar{p} = \frac{1}{V} \int_V \left[\frac{1}{V_f} \int_{V_f} p \, \mathrm{d}V \right] \mathrm{d}V, \tag{22}$$

where V is the unit cell volume and V_f the volume of fluid contained within the unit cell. As discussed by Quintard and Whitaker [22], ordinary spatial phase average are not appropriate for ordered porous media, i.e. spatially periodic porous media. For this type of media, a macroscopic intrinsic variable, such as the pressure, must be defined in terms of cellular average. As explained by Quintard and Whitaker [22], the macroscopic velocity can be defined, however, in terms of phase average, Equation (21). Once the velocity and pressure fields are determined at pore level, spatial averaging of these fields are performed according to Equations (21) and (22) and the permeability can be determined from Equation (20). It was found $k/d^2 = 0.048$ for model porous medium I and $k/d^2 = 0.011$ for model porous medium II. It is interesting to note that the staggered cylinder arrangement (model II) leads to a reduction of the permeability by a factor 5 compared with the square array (model I).

4.4. Validity of macroscopic model

The simulations for evaluating the validity of the macroscopic model, equations (1)–(3), were performed for the following initial conditions: $p_0 = 10^5$ Pa; $\rho_0 = 1.27$ kg m^{-3} and $T_0 = 273.13$ K with air as gas. Two depressurisation laws were used, Bouhouch [18], a linear one and the law

$$f(t) = p_0 - \frac{p_0 - p_f}{2}(1 - \cos(\pi t/\tau)) \quad \text{with } \tau = 750 \ \mu\text{s}.$$

As both laws lead to the same main results, only the results obtained with the cosine law are reported in the present paper. Two pore sizes were considered, $d = 10$ μm (case 1) and $d = 100$ μm (case 2). The main characteristics of the pore level simulations are summarised in Table I. Simulations were run on a IBM RISC 6000/375 workstation. Typical CPU time was 5 s per

Table I. Main characteristics of the pore level simulations

	d (μm)	Δx (μm)	Δt (s)	Number of iterations	Reynolds	Mach	$p_0 - p_f$ (Pa)
Case 1	10	0.5	0.15×10^{-8}	250 000	≤ 0.62	$\leq 2 \times 10^{-4}$	10 000
Case 2	100	5	0.15×10^{-7}	50 000	≤ 0.62	$\leq 2 \times 10^{-4}$	5000

time step (this leads to rather intensive CPU times, over 70 h for instance for case 2). Note the low values of the maximum Reynolds and Mach numbers in Table I. This is consistent with the application that motivated the present study, Bouhouch *et al.* [7]. As a consequence of the depressurisation process, the temperature decreases within the domain, Figure 10. However, the temperature variation is only of 4 K, therefore, the authors conclude that the effect of temperature variations can be safely ignored in the comparison between the results of the macroscopic model, which does not take into account thermal transfers, and the results of the pore level simulations.

Figure 11 compares the evolution of the pressure difference obtained for case 2 and model porous medium II by cellular averaging the microscopic results and on the other hand by solving the problem directly at the macroscopic level, Equations (1)–(3). The pressure difference represented in Figure 11 is defined as the difference between the pressure at the outlet and the pressure at $x = 0$. As can be seen from Figure 11, there is a discrepancy between

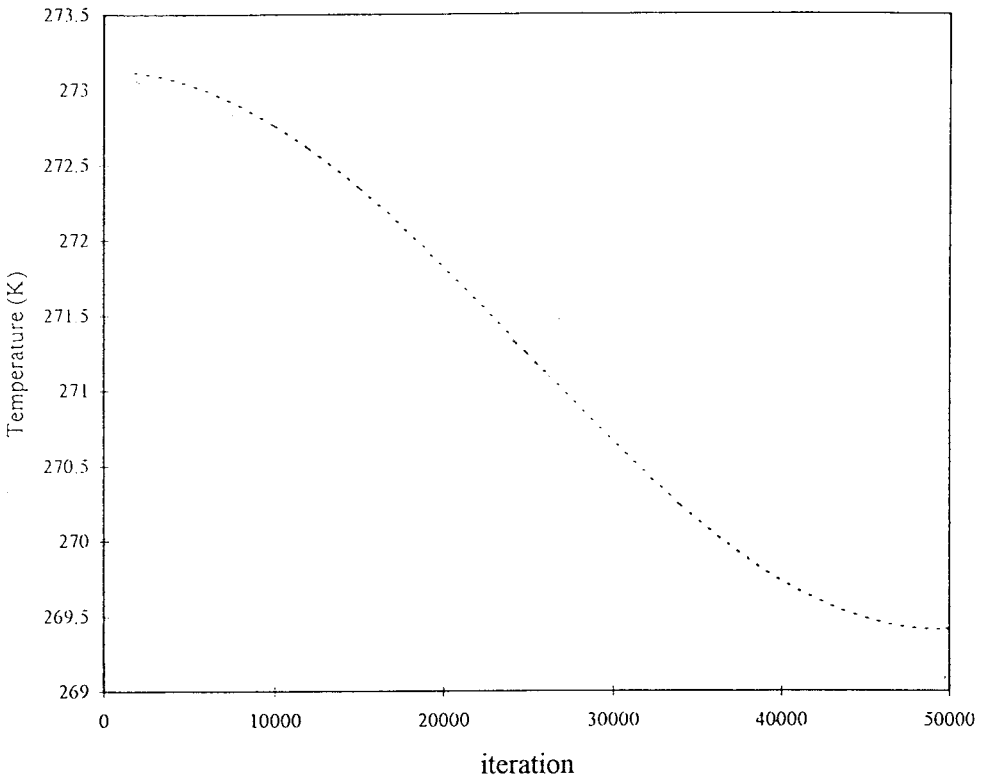

Figure 10. Average temperature variation within the pore space during depressurisation (iteration = time step).

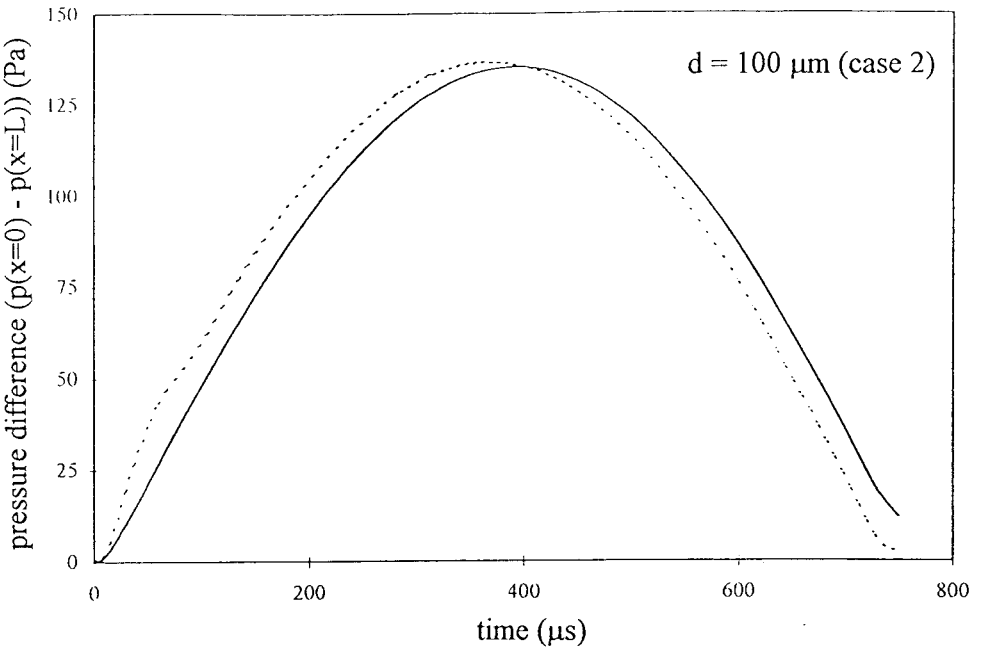

Figure 11. Pressure difference as a function of time (case 2, model porous medium II). Solid line: macroscopic model, dashed line: cellular averaged microscopic pressure.

the cellular averaged pressure difference and the pressure difference predicted by means of the macroscopic model. On the contrary, for case 1, which is shown in Figure 12, the discrepancy is very small. Similar results are obtained in terms of macroscopic velocities or for model porous medium I, Bouhouch [18]. Thus, the macroscopic model leads to good predictions for case 1 and much less good predictions for case 2. This can be illustrated by computing the evolution of the local permeability from the microscopic data for cases 1 and 2. Assuming Darcy's law, the apparent permeability k_a as a function of space and time was computed as described before, Equation (20). As can be seen from Figure 13, k_a is quasi-independent of x except at the very beginning of the process. The time evolution of the k_a is shown in Figure 14 for cases 1 and 2. As can be seen from Figure 14, k_a is significantly different from the intrinsic or steady state permeability k during most of the depressurisation process for case 2. On the contrary, k_a rapidly tends towards k for case 1. The results displayed in Figure 14 were obtained for model porous medium II. Similar results were obtained for model porous medium I.

5. DISCUSSION

As the apparent permeability is significantly different from the intrinsic permeability for case 2, it is expected that the pore level flow structure for case 2 presents striking differences compared with the stationary flow structure associated with an incompressible Stokes flow at pore level (see Figure 9 for model porous medium I). This is illustrated in Figure 15, which shows an example of the flow structure for case 2 and model porous medium I. Recirculating eddies can be observed in Figure 15. Their structure, however, is quite different from the

structure corresponding to the incompressible steady creeping flow, Figure 9. On the contrary for case 1, Figure 16, the flow structure is very close to the flow structure of the incompressible steady creeping flow. This indicates that a local steady state regime is reached during most of the depressurisation process for case 1, while the regime is essentially locally not established for case 2. This explains the discrepancies observed between case 1 and case 2 in terms of pressure difference, Figure 11. Physically these differences can be interpreted in terms of time scales. As the Reynolds number and the Mach number are small in these numerical experiments, the two phenomena controlling the process are in fact,

– the local viscous relaxation
– the diffusion of the pressure over the domain

The characteristic time scales associated with these two phenomena may be defined respectively as

$$t_{\text{vis}} = \frac{d^2\rho}{\mu}, \tag{23}$$

$$t_{\text{pr}} = \frac{L^2\mu\varepsilon}{kP}. \tag{24}$$

It is interesting to compare these time scales to the time scale τ associated with the imposed external pressure variations, i.e. 750 μs. The results are summarised in Table II. As can be seen from Table II, the steady state regime may be considered as reached locally for case 1 since $t_{\text{vis}} \ll \tau$ but not for case 2. This is fully consistent with the pore level flow structures discussed above. It can also be noted that Bouhouch [18] did a similar study for a repressurisation process and not surprisingly reached the same conclusions as the ones reported in the present paper.

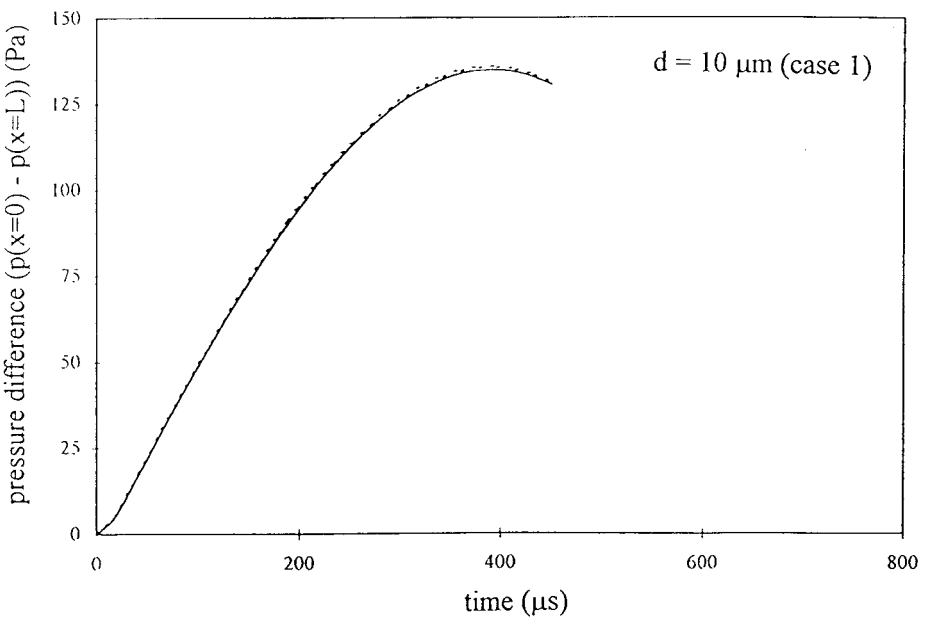

Figure 12. Pressure difference as a function of time (case 1, model porous medium II). Solid line: macroscopic model, dashed line: cellular averaged microscopic pressure.

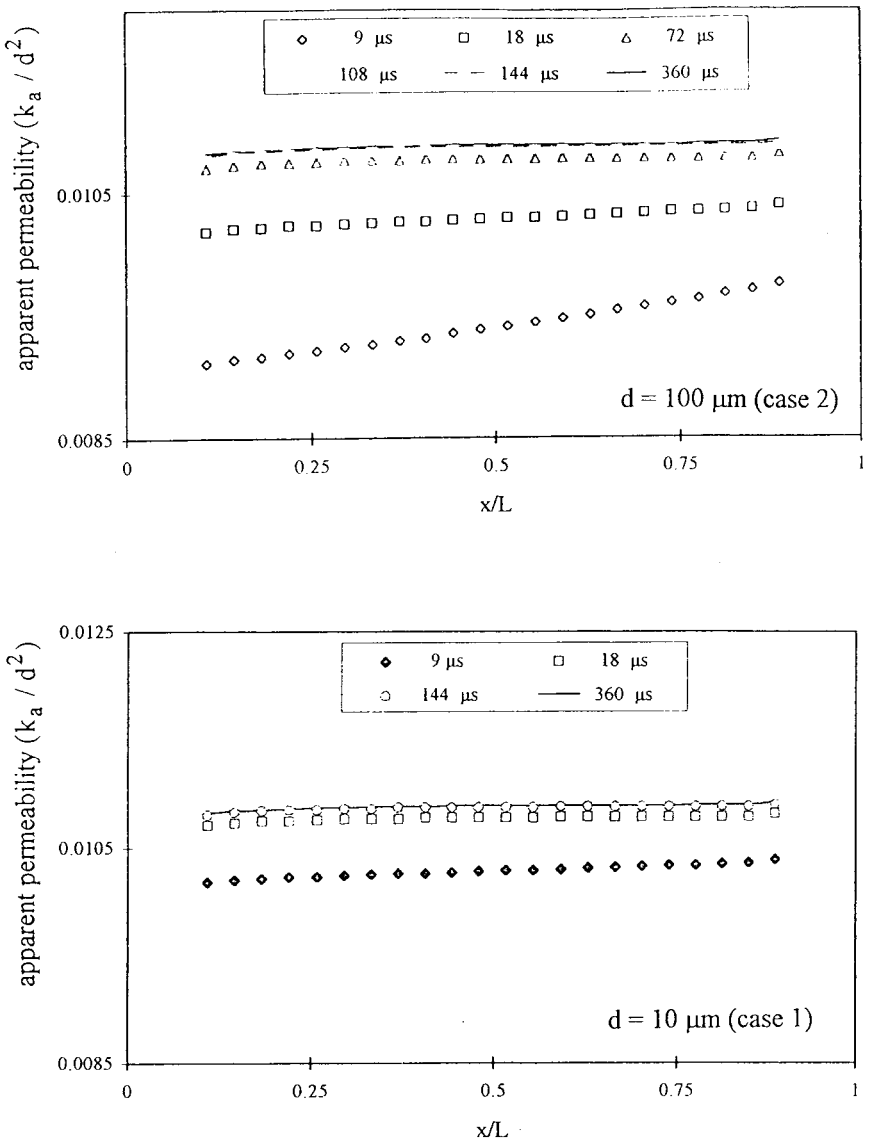

Figure 13. Spatial evolution of apparent permeability for case 1 and case 2 (model porous medium II).

When $t_{vis} \ll \tau$ and $t_{pr} \ll \tau$, the macroscopic model can in fact be simplified. As the pressure diffuses very rapidly compared with the typical time scale of the external pressure variation, the pressure within the porous medium is in fact quasi-uniform and equal to the external pressure. In this case, the transient term in Equation (3) can be neglected and the evolution of the mass flow rate as a function of time can be simply determined from a macroscopic mass balance over the whole porous domain.

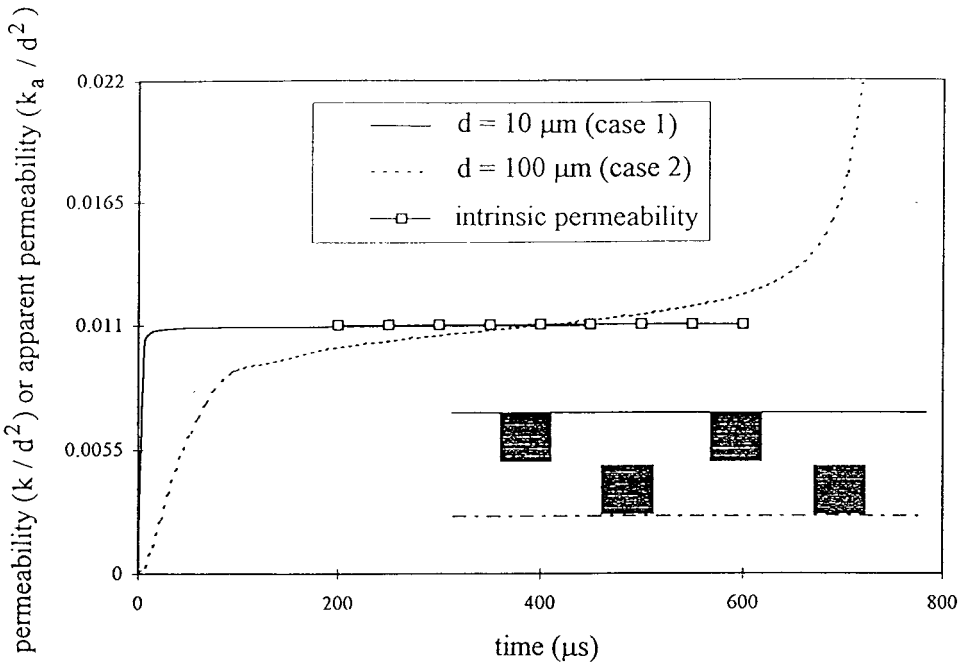

Figure 14. Apparent permeability as a function of time (model porous medium II).

6. CONCLUDING REMARKS

In this paper, a quasi-isothermal variable density flow in porous medium was studied from simulations of the flow at pore level. The flow was due to a depressurisation process

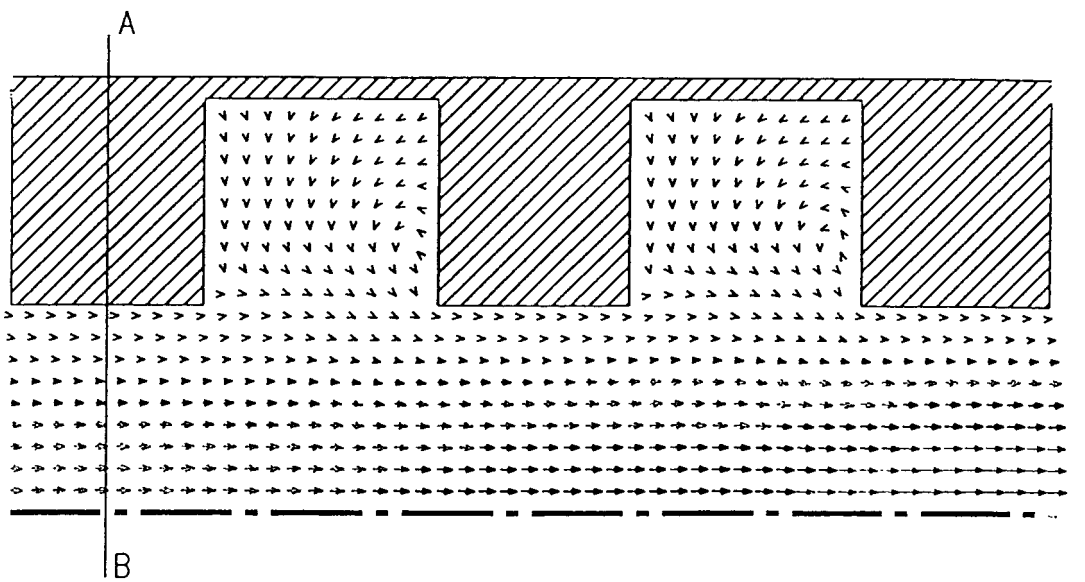

Figure 15. Example of pore level flow structure for case 2 and model porous medium I.

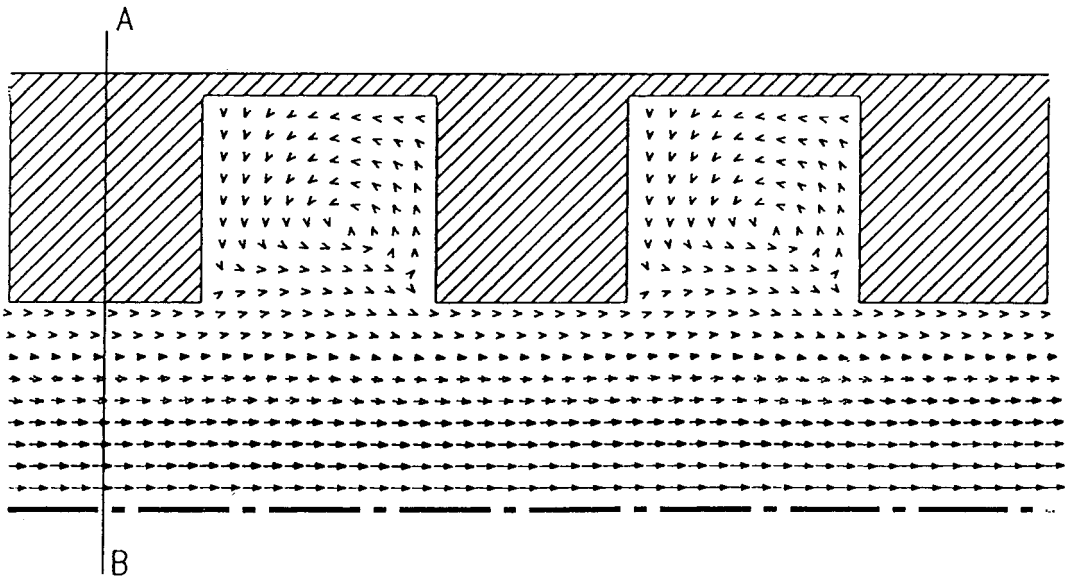

Figure 16. Example of pore level flow structure for case 1 and model porous medium I.

propagating through pore space. Under the constraint of low Reynolds and Mach numbers, it is found that the classic macroscopic model, which is based on Darcy's law, give good results provide the pore level viscous relaxation time scale is small enough compared with the characteristic time associated with the imposed pressure variation at the outlet of the domain. If this time scale separation is not satisfied, the flow is never established at the pore level and the apparent permeability significantly differs from the intrinsic permeability of the medium. In that case, according to Auriault *et al.* [4], the process is not homogenisable, i.e. an equivalent macroscopic description cannot be found. Finally, it should be stressed that the situation studied in the present paper is one of the simplest that can be considered in terms of compressible flow in porous media. Macroscopic models developed for more involved situations (greater Mach number with significant heat transfer for example) are essentially phenomenological. Pore level simulations seems to be a promising approach to assess the validity or the domain of validity of these models.

Table II. Time scale values

	t_{vis} (μs)	t_{pr} (μs)	τ (μs)
$d = 10$ (μm) (case 1)	7.4	18.5	750
$d = 100$ (μm) (case 2)	740	18.5	750

ACKNOWLEDGMENTS

Financial supports from CNES (Centre National d'Etudes Spatiales) and ESA (European Space Agency) are gratefully acknowledged. Special thanks are due to A. Kourta for valuable discussions. A.B. was supported by a BDI grant from CNRS and CNES.

REFERENCES

1. A.E. Scheidegger, *The Physics of Flow Through Porous Media*, University of Toronto Press, Toronto, 1974.
2. A. de Ville, 'On the properties of compressible gas flow in a porous media', *Transp. Porous Media*, **22**, 287–306 (1996).
3. C.A. Kodres, 'Flow parameter approach to modelling the flow of heated gases through high resistance porous media', *Transp. Porous Media*, **15**, 229–249 (1994).
4. J.L. Auriault, T. Strzelecki, J. Bauer and S. He. 'Porous deformable media saturated by a very compressible fluid: quasi-statics', *Eur. Mech. A/S*, **9**, 373–392 (1990).
5. M. Sozen and K. Vafai, 'Analysis of oscillating compressible flow through a packed bed', *Int. J. Heat Fluid Flow*, **12**, 130–136 (1991).
6. N.S. Raghavan, M.M. Hassan and D.M. Ruthven, 'Numerical simulation of PSA system', *A.I. Ch. E. J.*, **31**, 385 (1985).
7. A. Bouhouch, M. Prat and S. Bories, 'Transient compressible flow and thermal transfer within a heterogeneous porous system', *AIAA J. Thermophys. Heat Transf.*, **9**, 144–150 (1995).
8. R.P. Sheeve, 'Supersonic flow from a porous metal plate', *AIAA J.*, **6**, 752–753 (1968).
9. G. Emanuel and J.P. Jones, 'Compressible flow through a porous plate', *Int. J. Heat Mass Transf.*, **11**, 827–836 (1968).
10. D.A. Nield. 'Modelling high speed flow of a compressible fluid in a saturated porous media', *Transp. Porous Media*, **14**, 85–88 (1994).
11. D.L. Johnson, J. Koplick and R. Dashen, 'Theory of dynamic permeability and tortuosity in fluid-saturated porous media', *J. Fluid Mech.*, **176**, 379–402 (1987).
12. E. Sanchez-Palencia, 'Non-homogeneous media and vibration theory', *Lecture Notes in Physics* 127, Springer, Berlin, 1980.
13. M. Prat, 'On the boundary conditions at the macroscopic level', *Transp. Porous Media*, **4**, 258–280 (1989).
14. M. Prat, 'Some refinements concerning the boundary conditions at the macroscopic level', *Transp. Porous Media*, **7**, 147–161 (1992).
15. R.I. Issa, 'Solution of the implicitly discretised fluid flow equations by operator-splitting', *J. Comput. Phys.*, **62**, 40–65 (1986).
16. S.V. Patankar, *Numerical Heat Transfer and Fluid Flow*, Hemisphere, 1980.
17. J.H. Ferziger and M. Peric, *Computational Method for Fluid Dynamics*, Springer, Berlin, 1996.
18. A. Bouhouch, 'Modélisation des écoulements monophasiques et des transferts de chaleur en milieux poreux. Situations transitoires à masse volumique variable et à haute température', *I.N.P.T. Thesis*, 1996.
19. T.J. Poinsot and S.K. Lele, 'Boundary conditions for direct solutions of compressible viscous flows', *J. Comp. Phys.*, **101**, 104–129 (1992).
20. N. Hannoun, H.C. Boisson and A. Ben Abdessalam, 'Open boundary conditions for an implicit compressible Navier–Stokes solver', *Proc. 8èmes Journées Internationales de Thermique*, **2**, 47–54 (1997).
21. J.L. Higdon, 'Stokes flow in arbitrary two-dimensional domains: shear flow over ridges and cavities', *J. Fluid Mech.*, **159**, 195–226 (1985).
22. M. Quintard and S. Whitaker, 'Transport in ordered and disordered porous media: volume-averaged equations, closure problems, and comparison with experiment', *Chem. Eng. Sci.*, **48**, 2537–2564 (1993).

